Magnetization and spin-flip Raman scattering in $Cd_{1-x}Cr_xSe$ and $Cd_{1-x}V_xSe$

X. Lu, I. Miotkowski, S. Rodriguez, and A. K. Ramdas

Department of Physics, Purdue University, West Lafayette, Indiana 47907, USA

H. Alawadhi

Department of Applied Physics, University of Sharjah, United Arab Emirates

T. M. Pekarek

Department of Physics, University of North Florida, Jacksonville, Florida 32224, USA

Spin-flip Raman scattering (SFRS) from donor-bound electrons in II-VI diluted magnetic semiconductors (DMSs) containing $3d$ transition-metal ions, e.g., $Cd_{1-x}Cr_xSe$ and $Cd_{1-x}V_xSe$, allows one to explore the exchange interaction between the conduction band or donor electrons with the $3d$ magnetic ions, which is the so-called s-d exchange interaction. The s-d exchange energy, being the SFRS Raman shift after subtracting the intrinsic Zeeman splitting characterized by $g^* = 0.52$ for CdSe, together with the magnetization measurements of those DMSs, allow one to deduce the s-d exchange constant $N_0\alpha$. For $Cd_{1-x}Cr_xSe$ and $Cd_{1-x}V_xSe$, the $N_0\alpha$ values are 210 ± 13 and 269 ± 10 meV, respectively.

PACS number(s): 78.30.−j, 78.20.Ls, 78.55.Et

I. INTRODUCTION

II-VI semiconductors in which $3d$ transition-metal ions ($3d$ TMIs) are incorporated resulting in diluted magnetic semiconductors (II-VI DMSs) have been the focus of intense research thanks to the coexistence of semiconductor and magnetic phenomena, resulting from the so-called sp-d exchange interaction between the band carriers and localized electrons of the magnetic ions.[1] Theoretical investigations[2,3] predict that the p-d exchange interaction in II-VI DMSs with $3d$ transition-metal ions having less than a half-filled $3d$ shell (e.g., Sc, Ti, V, and Cr) are ferromagnetic, which is in striking contrast to the antiferromagnetic character of those having a half-filled (e.g., Mn) or more than a half-filled (e.g., Co, Fe, Ni, and Cu) $3d$ shell. This ferromagnetic p-d exchange interaction has been confirmed experimentally in several Cr-based DMSs[4–7] on the basis of magnetoreflectivity measurements. Mac *et al.*[8] also report a ferromagnetic p-d exchange interaction in $Cd_{1-x}V_xS$ as deduced from the Zeeman effect of the excitonic reflectivity and luminescence. The distinct varieties of magnetism displayed by TMIs continue to provide a strong motivation for synthesizing and studying such DMSs. The magnetism displayed by a given TMI is intimately related to its localized magnetic moment influenced by its internal electronic level structure as a constituent of the nonmagnetic host lattice. As a result, Mn- and Co-based DMSs show paramagnetism which follow $B_{5/2}$ and $B_{3/2}$ Brillouin functions, respectively;[1,9] Fe-based DMSs, however, exhibit the van-Vleck-type paramagnetism.[9–11] For V-based DMSs, e.g., $Cd_{1-x}V_xTe$, the magnetization follows a $B_{3/2}$ Brillouin function. However, Cr-based DMSs display a paramagnetism[4,12–15] that is intermediate between the Brillouin type and van Vleck type. In V- and Cr-based DMSs, the ferromagnetic sp-d exchange interaction may also mediate the ferromagnetic coupling between the magnetic ions via d-d exchange interaction. Indeed, room-temperature ferromagnetism of $Zn_{1-x}Cr_xTe$ film with $x = 0.2$ has been

reported[16,17] and has received notice in connection with potential spintronic[18] applications.

Due to the small concentrations in which V and Cr can be incorporated in DMSs, with correspondingly small excitonic Zeeman splittings, not all of the excitonic Zeeman lines are resolved in magnetoreflectivity measurements. As a result, the sp-d exchange interaction constants $N_0\alpha$ and $N_0\beta$ cannot be deduced separately in those measurements, but rather only the difference $(N_0\alpha - N_0\beta)$ can be evaluated.[4–7] The value $(N_0\alpha - N_0\beta)$ was found to be negative for all of the Cr-based DMSs studied so far, in contrast to the positive values for Mn-, Co-, and Fe-based DMSs.[9] With the assumption that $N_0\alpha$ for Cr-based DMSs is about 0.2 eV, which is reasonable and indeed is the case for Mn-, Co-, and Fe-based DMSs reported so far, $N_0\beta$ is deduced to be positive for Cr-based DMSs. All of the experimental evidence thus points to a ferromagnetic p-d exchange interaction in Cr-based II-VI DMSs. A direct measurement of $N_0\alpha$ is thus important. Resonantly enhanced excitonic spin-flip Raman scattering (SFRS) offers an opportunity to determine the magnitude *and* sign of $N_0\alpha$ accurately, even for DMSs with very low TMI concentrations, as demonstrated in zinc blende $Cd_{1-x}V_xTe$.[19] In the present study, we report and discuss SFRS in $Cd_{1-x}Cr_xSe$ and $Cd_{1-x}V_xSe$ that have a wurtzite structure.

II. EXPERIMENT

$Cd_{1-x}Cr_xSe$ and $Cd_{1-x}V_xSe$ crystals were grown using the modified vertical Bridgman technique with nominal Cr and V concentrations of $\leqslant 2\%$ due to their low solubility. The crystallographic direction of the $\hat{\mathbf{c}}$ axis of these crystals was determined from their x-ray Laue pictures. Wavelength-modulated reflectivity (WMR) spectra were obtained at low temperatures in the zero magnetic field. The technique for obtaining WMR is discussed in detail in Ref. 20. Photoluminescence (PL) and Raman spectra were recorded with a photon-counting detection system incorporating a cooled photomultiplier, following
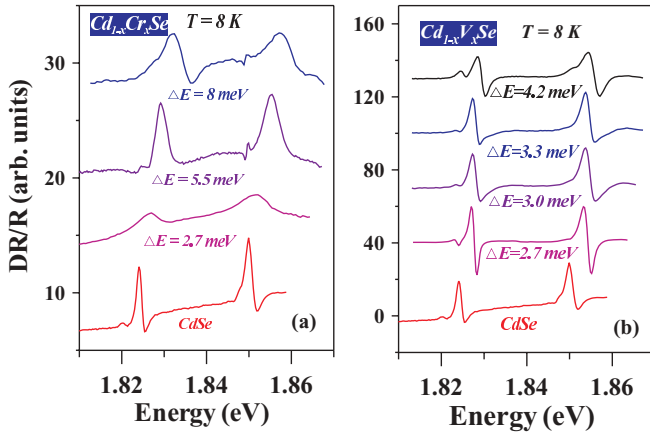
FIG. 1. (Color online) Wavelength-modulated reflectivity spectra: (a) $Cd_{1-x}Cr_xSe$ and (b) $Cd_{1-x}V_xSe$. The two signatures correspond to exciton A (lower energy) and exciton B (higher energy), respectively.

the spectral analysis with a double-grating monochromator. A third grating operated in tandem is often necessary for a more rigorous rejection of the parasitic radiation close to the incident laser energy. An optical cryostat incorporating a superconducting magnet was employed for applying magnetic fields up to 6 T and for achieving temperatures as low as 1.8 K. Raman spectra were excited with a tunable Coherent CR699 ring dye laser using DCM [2-[2-4-(dimethylamino) phenyl]-6-methyl-4H-pyran-4-ylidene]-propanedinitrile as the dye. The magnetization was measured in magnetic fields up to 7 T, employing a Quantum Design MPMS XL7 superconducting quantum interference magnetometer.

III. RESULTS AND DISCUSSION

A. WMR spectra

WMR spectra of $Cd_{1-x}Cr_xSe$ and $Cd_{1-x}V_xSe$ ternary alloys as a function of x are shown in Figs. 1(a) and 1(b), respectively, where A and B excitonic signatures are clearly observed. The excitonic features for the three $Cd_{1-x}Cr_xSe$ specimens shift with increasing x by 2.5, 5.2, and 7 meV with respect to the corresponding features for CdSe, while those for the available $Cd_{1-x}V_xSe$ specimens shift by 2.7 to 4.2 meV with respect to that of CdSe. Both Figs. 1(a) and 1(b) indicate that $Cd_{1-x}Cr_xSe$ and $Cd_{1-x}V_xSe$ ternary alloys with good optical quality have resulted in the crystal growth.

B. Magnetization and its relation with *s-d* exchange energy

Villeret *et al.*[21] have systematically investigated the low-lying electronic levels of transition-metal ions (TMIs) with the $3d^n$ electronic configuration, $n = 1$ to 9, in II-VI DMSs with either the zinc-blende or the wurtzite structure. The electronic configurations for Cr^{3+}, Cr^{2+}, and Cr^+ are $3d^3$, $3d^4$, and $3d^5$, respectively, with the corresponding lowest terms ^4F ($L = 3$, $S = 3/2$), ^5D ($L = 2$, $S = 2$), and $^6S_{5/2}$ ($S = 5/2$, $L = 0$). The energy level schemes for Cr^{3+}, Cr^{2+}, and Cr^+ in II-VI DMSs when subjected to the crystal field, spin-orbit interaction, and Jahn-Teller effect (for Cr^{3+} and Cr^{2+} only) have been described in detail in our previous
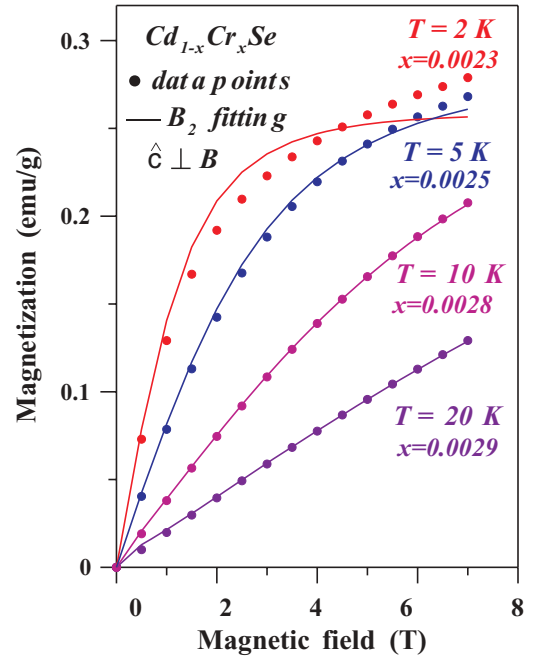

FIG. 2. (Color online) Magnetization of $Cd_{1-x}Cr_xSe$, after subtracting the diamagnetism of the host, as a function of B at several temperatures. The full circles are experimental data and the solid lines are the fitting of the magnetization with B_2 Brillouin function, and $x \sim 0.003$.

paper.[22] Since the ground state of Cr^{2+} in the II-VI DMSs, e.g., in ZnTe and CdTe, is a singlet,[23,24] yet with magnetic excited states close enough for it to acquire a magnetic moment by mixing, the magnetization of Cr^{2+} exhibits properties intermediate between a van-Vleck-type and a Brillouin-type paramagnetism. However, consistent with the quenching of the orbital moments, the magnetization of Cr^{2+} in Cr-based DMSs[14,15,25] can be approximately fitted with a B_2 Brillouin function. The x values of the three $Cd_{1-x}Cr_xSe$ specimens used to obtained Fig. 1(a), deduced by fits to the magnetization with a B_2 Brillouin function, are approximately 0.001, 0.002, and 0.003. In Fig. 2, the magnetization of $Cd_{1-x}Cr_xSe$ specimens, measured in Fig. 1(a), as a function of B, with $x \sim 0.003$. At low temperatures (e.g., 2 K), the magnetization of $Cd_{1-x}Cr_xSe$ saturates at high B, in contrast to the absence of saturation expected for van Vleck paramagnetism[10,11] at lowest T (2 K) and highest B (6 T). However, the approach to saturation as a function of B at low temperatures is more gradual than that for the B_2 Brillouin function; in other words, the magnetism of Cr-based DMSs is between van-Vleck-type and Brillouin-type paramagnetism. To the extent that the fits for magnetization with B_2 are not exact at 2 and 5 K, the x values deduced should be considered as nominal.

Besides the Cr^{2+} (see Refs. 4,12–15,24–26) charge state, Cr^+ and Cr^{3+} have also been reported in II-VI DMSs in microwave electron paramagnetic resonance (EPR).[27–36] While the observed signature of SFRS in $Cd_{1-x}Cr_xSe$ is clearly related to Cr^{2+}, we did not observe Raman-EPR features associated with Cr^+. However, Raman-EPR signatures of Cr^+ in $Zn_{1-x}Cr_xTe$ and $Cd_{1-x}Cr_xTe$ were reported by us,[22] but not for the spin-flip Raman scattering (SFRS) from donor-bound

electrons. The reason may be related to crystal-growth conditions which determine whether the host semiconductor is a p or n type; it is well known that as-grown CdSe is an n type due to Se vacancies, while CdTe is a p type due to Cd vacancies. In $Zn_{1-x}Cr_xTe$ and $Cd_{1-x}Cr_xTe$, a small fraction of Cr^{2+} transforms into Cr^+ acceptors by capturing an additional electron from the "anonymous" donors, and thus displays Raman-EPR of Cr^+, but leaving insufficient neutral donors for observing spin-flip Raman scattering. However, in $Cd_{1-x}Cr_xSe$, it appears that no Cr^+ occurs as the absence of Raman-EPR of Cr^+ shows, whereas the observation of SFRS is evidence for the presence of neutral donors. It is not clear why no EPR and Raman-EPR of Cr^{2+}, Cr^+, and Cr^{3+} in $Cd_{1-x}Cr_xSe$ have been reported.

Vanadium in II-VI DMSs also occurs in V^{3+}, V^{2+}, and V^+ charge states, as observed in EPR[37–40] and optical measurements.[41–43] It was also found that V^{3+} can be photoconverted into V^{2+} with the light of an appropriate photon energy. The electronic configurations for V^{3+}, V^{2+}, and V^+ are $3d^2$, $3d^3$, and $3d^4$, respectively, with the corresponding lowest terms ^3F ($L = 3$, $S = 1$), ^4F ($L = 3$, $S = 3/2$), and ^5D ($L = 2$, $S = 2$). V^{2+} (V^+) has the same electronic configuration as Cr^{3+} (Cr^{2+}), and thus can be expected to display a similar internal energy-level structure. When subjected to the crystal field and spin-orbit interaction, V^{3+} is expected to display an isotropic paramagnetic behavior described by a B_1 Brillouin function.[19] V^{2+} (Cr^{3+}) and V^+ (Cr^{2+}) are subjected to a static Jahn-Teller distortion, and the magnetization of V^{2+} (Cr^{3+}) can be well described by $B_{3/2}$, while that of V^+ (Cr^{2+}) can be approximately described by B_2. Since the magnetization of $Cd_{1-x}V_xSe$ after subtracting the diamagnetic contribution of the host, as shown in Fig. 3, can be quite precisely fitted

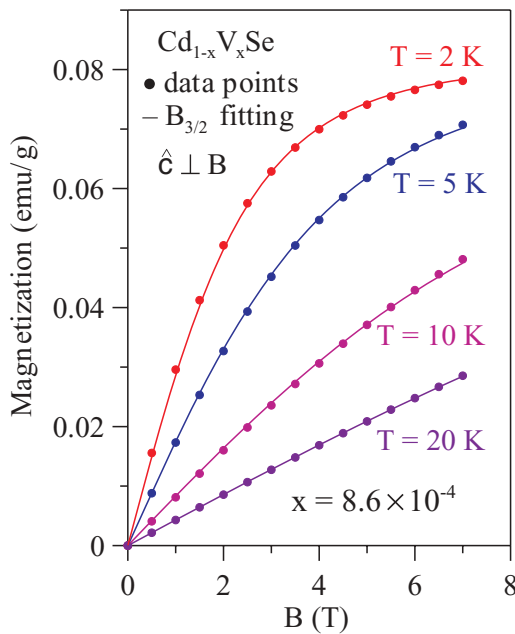with a $B_{3/2}$ Brillouin function, we conclude that a significant majority of the vanadium ions in $Cd_{1-x}V_xSe$ is in the V^{2+} charge state. The x value thus deduced with a $B_{3/2}$ fit in Fig. 3 yields the same number (8.6×10^{-4}) as deduced from the data at four different temperatures. Even though the vanadium concentration incorporated in CdSe is very small, it is sufficient to observe SFRS from donor-bound electrons in $Cd_{1-x}V_xSe$ under resonant conditions.

The Raman shift of SFRS from donor-bound electrons in DMSs is given by[19,44]

$$\hbar\omega_{SFRS} = g^*\mu_B B - x\alpha N_0\langle\langle S_z\rangle\rangle, \quad (1)$$

where g^* is the intrinsic g factor of the host crystals (CdSe in this case), x is the concentration of magnetic ions (e.g., Cr), $N_0\alpha$ is the s-d exchange constant between the delocalized electrons in the conduction band or donor-bound electrons in large effective mass orbits, on the one hand, and the localized magnetic ions, on the other, and $\langle\langle S_z\rangle\rangle$ is the thermal and spatial average of the magnetic ion spin projection along the direction of the external magnetic field. $\langle\langle S_z\rangle\rangle$ can be expressed in terms of macroscopic magnetization M_m^* (Ref. 9) as

$$M_m^* = -\frac{g_S\mu_B N_A}{W(x)}x\langle\langle S_z\rangle\rangle, \quad (2)$$

where N_A is the Avogadro's number, $W(x)$ is the molar weight of the DMS, and g_S is the g factor of the magnetic ion. M_m^* can be deduced from the measured magnetization M_m after subtracting the diamagnetic contribution of the host, $M_m^* = M_m - \chi_{dia}H$. Equation (1) thus becomes

$$\hbar\omega_{SFRS} = g^*\mu_B B + \alpha N_0\frac{W(x)}{g_S\mu_B N_A}M_m^*. \quad (3)$$

FIG. 3. (Color online) Magnetization of $Cd_{1-x}V_xSe$, after subtracting the diamagnetism of the host, as a function of B at several temperatures. The full circles are experimental data and the solid lines are the fitting of the magnetization with $B_{3/2}$ Brillouin function.
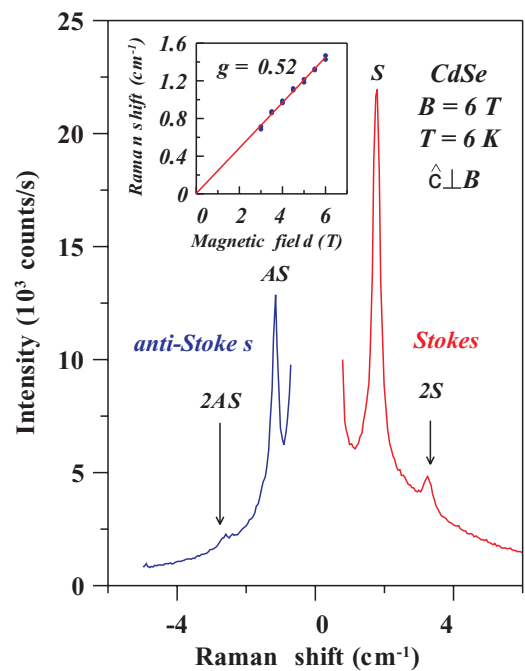

FIG. 4. (Color online) First- and second-order Stokes and anti-Stokes spin-flip Raman scattering (SFRS) from donor-bound electrons in CdSe recorded at 8 K and 6 T.

For $Cd_{1-x}Cr_xSe$, $g^* = 0.52$, as shown in the inset of Fig. 4, and $g_S = 1.887$ (see Ref. 25). The second term in Eq. (3) is called the *s-d* exchange energy, which is linear with respect to M_m^* and its linear least-squares fit yields the *s-d* exchange constant, $N_0\alpha$.

C. Spin-flip Raman scattering (SFRS) in CdSe, $Cd_{1-x}Cr_xSe$, and $Cd_{1-x}V_xSe$

Raman spectra were recorded in the backscattering geometry and a right-hand laboratory coordinate system ($\mathbf{h},\mathbf{k},\mathbf{v}$) defined by the magnetic field $\mathbf{B}$ along the horizontal ($\mathbf{h}$) direction as well as the direction of propagation of the incident light by $\bar{\mathbf{k}}$. Strong resonant Raman scattering, with the incident photon energy close to the excitonic band gap, is observed in the $\bar{\mathbf{k}}(\mathbf{hh})\mathbf{k}$ configuration with the mutually orthogonal $\mathbf{k}$, $\hat{\mathbf{c}}$, and $\mathbf{B}$. The Raman spectrum of CdSe recorded at $T = 8$ K and $B = 6$ T under an excitonic resonant condition is shown in Fig. 4. Stokes (S) and anti-Stokes (AS) Raman lines were observed with the Raman shift linear in magnetic field and independent of temperature over the range 2–10 K. Figure 4 also shows the second order of the Stokes (2S) and anti-Stokes (2AS) Raman features. The Raman lines are attributed to SFRS from donor-bound electrons, as discussed below. The SFRS Raman shift in an intrinsic CdSe is given by

$$\hbar\omega_{\text{SFRS}} = g^* \mu_B B, \tag{4}$$

where g^* is the intrinsic g factor, μ_B is the Bohr magneton, and B is the magnetic induction. The linear least-squares fit of the B dependence of the SFRS Raman shift, as shown in the inset of Fig. 4, yields $g^* = 0.52$, which is identical to that obtained by Henry *et al.*[45]

The PL spectrum of the same CdSe sample displays a strong peak (E_{PL}) at 1.82025 eV, whereas the *A*-exciton signature in the WMR measurements in Fig. 1(a) occurs at 1.8238 eV. We assign the former to an exciton bound to a shallow donor and the latter to the free *A* exciton; these values are consistent with those reported by Yu *et al.*[46] at 1.819 and 1.8231, respectively. Figure 5(a) shows the resonance profile of Stokes and anti-Stokes components of SFRS from donor-bound electrons in CdSe. Since the incident photon energy for resonance enhancement is around E_{PL}, it is reasonable to attribute the microscopic process of the spin-flip Raman transitions of donor-bound electrons as mediated via exciton *A* bound to a shallow neutral donor. The differential scattering cross section[47] can be written as

$$\frac{d\sigma}{d\Omega} \sim f^2 \left(\frac{e^2}{mc^2}\right)^2 \frac{\omega_s}{\omega_L} \frac{(\hbar\omega_L)^2}{(E_i - \hbar\omega_L)^2 + (\Gamma/2)^2}, \tag{5}$$

where f is the oscillator strength for an intermediate state at energy E_i, Γ is a phenomenological broadening parameter, and $\hbar\omega_L$ is the incident photon energy. As pointed out by Heiman *et al.*,[48] the bound exciton contributes much more than the free excitons since the oscillator strength for bound excitons is much larger, and the contribution from bound excitons *B* and *C* is neglected due to the energy range. Thus, only bound exciton *A* dominates in the above Raman process, which is consistent with the resonance enhancement occurring near E_{PL} associated with donor-bound exciton *A* in Fig. 5(a).
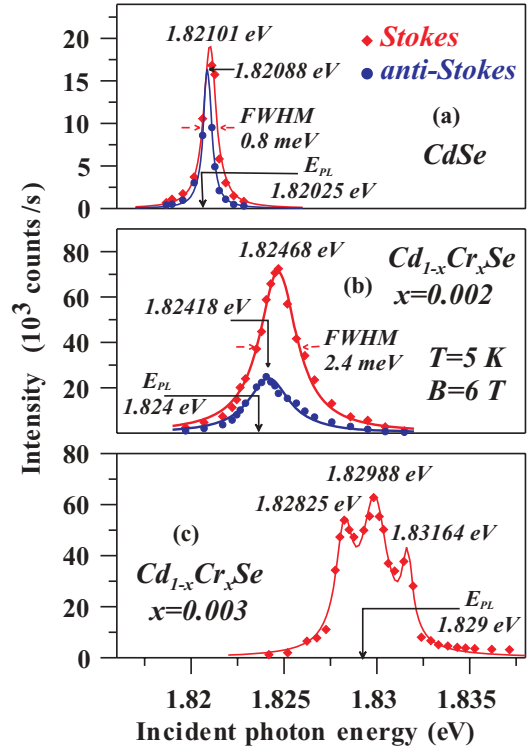

FIG. 5. (Color online) The intensities of the Stokes and the anti-Stokes Raman lines in $Cd_{1-x}Cr_xSe$ as a function of the incident photon energy, i.e., the resonance profiles, recorded at $T = 5$ K and $B = 6$ T. E_{PL} is the peak position of the photoluminescence (PL) spectrum. FWHM is the full width at half maximum.

Figure 6 shows the Raman spectrum in $Cd_{1-x}Cr_xSe$ with $x = 0.002$, recorded at 6 T and 5 K. The inset of Fig. 6 shows the x dependence of the Raman signature. The Raman shift of SFRS from donor-bound electrons in CdSe is 1.5 cm^{-1}, whereas the Raman signatures in $Cd_{1-x}Cr_xSe$ with $x = 0.002$ and 0.003 in Fig. 6 occur at 5.7 and 9.7 cm^{-1}, respectively. The Raman signature is also temperature and magnetic field dependent, as shown in Fig. 7. The intensity of the Stokes and the anti-Stokes Raman components in $Cd_{1-x}Cr_xSe$, recorded at 6 T and 5 K, as a function of the incident and scattered photon energy, i.e., the resonance profile, are shown in Figs. 5(b) and 5(c) for $x = 0.002$ and 0.003, respectively. As in the case of CdSe shown in Fig. 5(a), the resonant enhancement of the Raman signature in both $Cd_{1-x}Cr_xSe$ specimens occurs when the incident photon energy approaches the corresponding photoluminescence energy (E_{PL}) of the donor-bound exciton *A*. The x, T, and B dependence, together with the resonant profile of the Raman signature in $Cd_{1-x}Cr_xSe$, are clearly characteristics of Raman shifts due to the spin flip of shallow neutral donor-bound electrons. The solid curves in Fig. 5 are fits to the data using Eq. (5). The full width at half maximum (FWHM) of the resonant profile for $Cd_{1-x}Cr_xSe$ increases with x. As shown in Eq. (5), the scattering cross section is directly related to the intermediate state [energy E_i in Eq. (5)], i.e., one of the Zeeman states of an exciton *A* bound to a neutral donor. For CdSe, the Zeeman components of the bound exciton merge into a single broad band with a relatively small FWHM of 0.8 meV. With the increase of x, the separation of
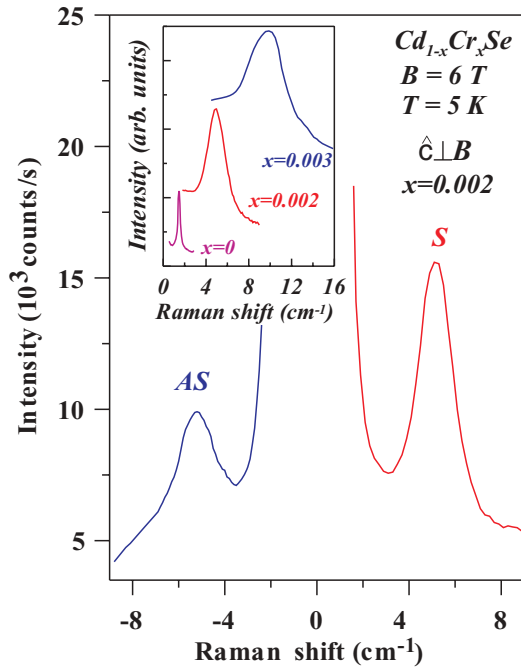
FIG. 6. (Color online) Raman spectrum of SFRS from donor-bound electrons in $Cd_{1-x}Cr_xSe$ recorded at $B = 6$ T and $T = 5$ K, displaying the Stokes (S) and anti-Stokes (AS) Raman lines. The inset shows the x dependence of the Stokes Raman shift.

FIG. 8. (Color online) The s-d exchange energy vs magnetization at $T = 2$ K for $Cd_{1-x}Cr_xSe$ ($x = 0.003$); the solid line is the linear least-squares fit.

the Zeeman components in $Cd_{1-x}Cr_xSe$ increase, resulting in the broader band for $x = 0.002$ with FWHM of 2.4 meV, and eventually evolves into three separate peaks for $x = 0.003$.

Figure 7 shows the s-d exchange energy, as well as M_m^*, for $Cd_{1-x}Cr_xSe$ as a function of the magnetic field at several temperatures. The s-d exchange energy versus magnetization
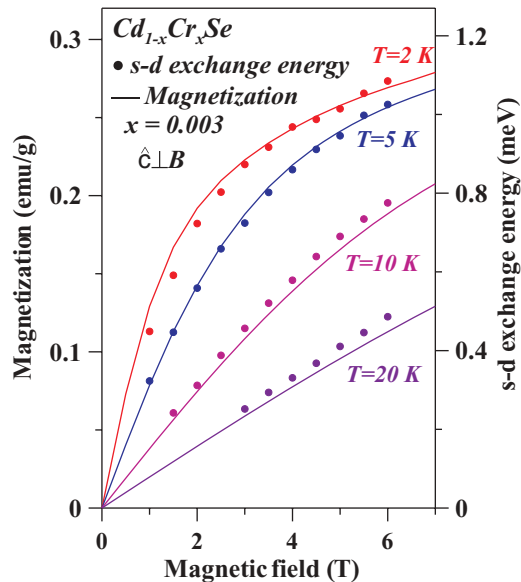

FIG. 7. (Color online) The s-d exchange energy (full circles), as well as magnetization (solid lines), after subtracting the host diamagnetism vs B plotted at $T = 2$, 5, 10, and 20 K for $Cd_{1-x}Cr_xSe$ ($x = 0.003$).
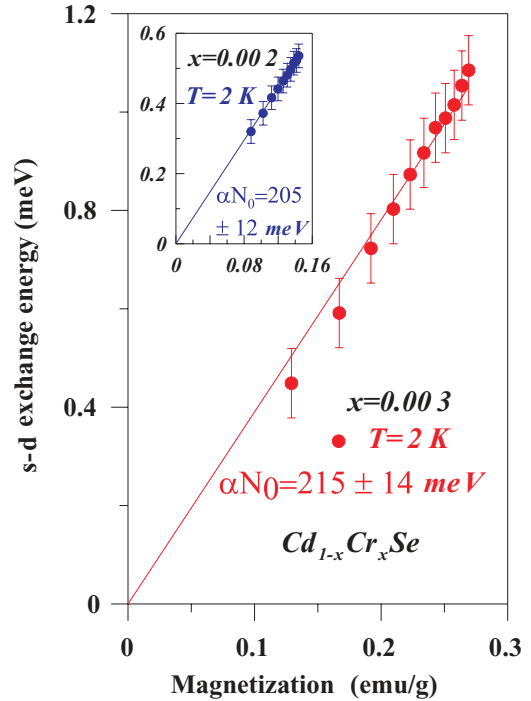
at 2 K is displayed in Fig. 8 for $x = 0.003$, and for $x = 0.002$ in the inset. The linear least-squares fit yields $N_0\alpha$ to be 215 ± 14 and 205 ± 12 meV, for $x = 0.003$ and 0.002, respectively. The average $N_0\alpha$ for $Cd_{1-x}Cr_xSe$ is thus 210 ± 13 meV, which is their value of $N_0\alpha$, 220 ± 20 meV, for $Cd_{1-x}Cr_xS$.

Figure 9 shows the Raman spectrum of SFRS in $Cd_{1-x}V_xSe$, recorded at 6 T and 5 K, and the inset shows its x dependence. The Raman shift of SFRS in $Cd_{1-x}V_xSe$ ($x = 8.6 \times 10^{-4}$) in Fig. 9 is 3.7 cm^{-1} at 6 T and 5 K, with 2.1 cm^{-1} attributed to the s-d exchange interaction and 1.5 cm^{-1} attributed to the intrinsic Zeeman splitting of CdSe. The PL spectra of $Cd_{1-x}V_xSe$ ($x = 8.6 \times 10^{-4}$) in Fig. 10(a) shows donor-bound excitonic features at 1.8230 eV, which is close to the incident photon energies for resonance enhancement in Fig. 10(b) for the Stokes at 1.8237 eV and for the anti-Stokes at 1.8232 eV. Thus the stronger resonance peaks are attributed to the SFRS mediated via an exciton A bound to a shallow neutral donor. The incident photon energies for the weaker resonance peaks in Fig. 10(b) for the Stokes at 1.8283 eV and for the anti-Stokes at 1.8276 eV are close to the A exciton of $Cd_{1-x}V_xSe$ ($x = 8.6 \times 10^{-4}$) in Fig. 1 at 1.8280 eV, thus we assign the weak features in Fig. 10(b) as SFRS mediated via a free exciton A. For the detailed microscopic mechanisms of the above Raman processes, we refer to Ref. 19.

Figure 11 shows the s-d exchange energy, as well as the magnetization, for $Cd_{1-x}V_xSe$ as a function of B at several temperatures. Both the s-d exchange energy and magnetization show saturation at high B and low T, which is characteristic of the Brillouin-type paramagnetism. For $Cd_{1-x}V_xSe$, we assume $g_S = 2$ (Ref. 19) in Eq. (3) since the exact value for V in CdSe is not available at the present time. The s-d exchange

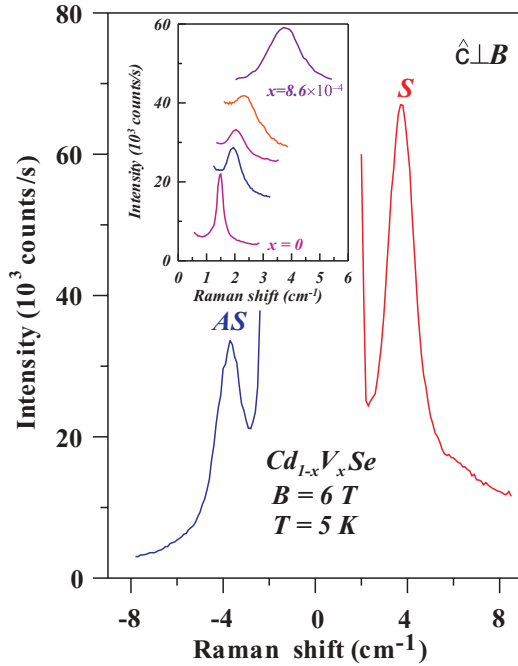FIG. 9. (Color online) Raman spectrum of SFRS from donor-bound electrons in $Cd_{1-x}V_xSe$ recorded at $B = 6$ T and $T = 5$ K. The Stokes (S) and anti-Stokes (AS) Raman lines are shown. The inset shows the x dependence of the Stokes Raman shift.

energy versus magnetization at 2 K is plotted in Fig. 12, and the linear least-squares fit yields the s-d exchange constant
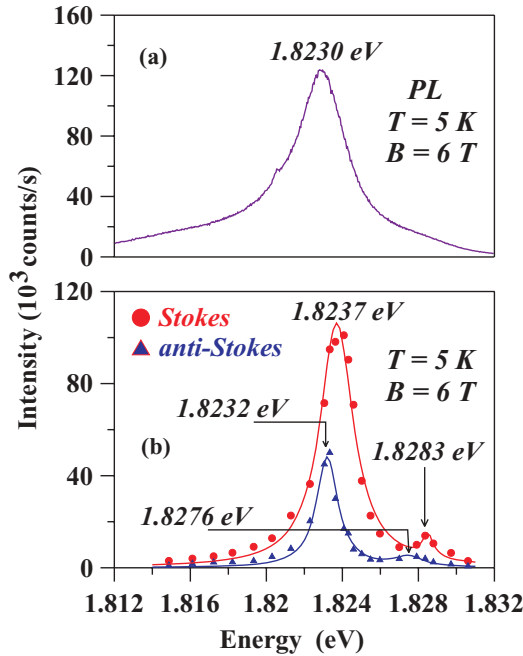

FIG. 11. (Color online) The s-d exchange energy (full circles, squares, and triangles), as well as magnetization (solid lines) after subtracting the host diamagnetism vs B plotted at $T = 2, 5, 10$, and 20 K for $Cd_{1-x}V_xSe$ ($x = 0.003$).

in $Cd_{1-x}V_xSe$, $N_0\alpha$, to be 269 ± 10 meV, in good agreement with the value 285 ± 8 meV in $Cd_{1-x}V_xTe$ (Ref. 19). Notice that the $N_0\alpha$ values for V in $Cd_{1-x}V_xSe$, 269 ± 10 meV, and in $Cd_{1-x}V_xTe$, 285 ± 8 meV, are larger than those for Cr in $Cd_{1-x}Cr_xSe$ in this report, 210 ± 13 meV, in $Cd_{1-x}Cr_xS$ reported by Twardowski *et al.*,[25] *viz.* 220 ± 20 meV, which appears to indicate, in II-VI DMSs, that V has a stronger s-d exchange interaction than does Cr.

FIG. 10. (Color online) (a) Photoluminescence (PL) spectrum of $Cd_{1-x}V_xSe$ showing a strong donor-bound A-exciton feature. (b) The intensities of the Stokes and the anti-Stokes Raman lines as a function of the incident photon energy, i.e., the resonance profiles, recorded at $T = 5$ K and $B = 6$ T.
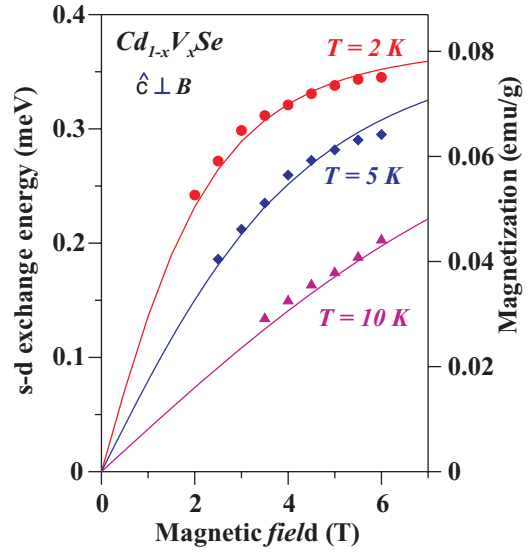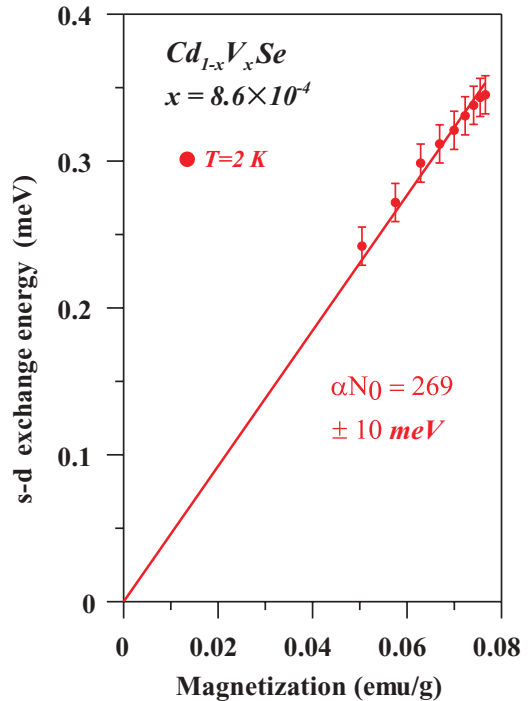

FIG. 12. (Color online) The s-d exchange energy vs magnetization at $T = 2$ K for $Cd_{1-x}V_xSe$ ($x = 0.003$); the solid line is the linear least-squares fit.

IV. CONCLUDING REMARKS

The accurate determination of $N_0\alpha$ in Cr-based II-VI DMSs plays an important role in deducing $N_0\beta$ and thus confirming their ferromagnetic character of the p-d exchange interaction.[4–7] The SFRS investigation has yielded $N_0\alpha$ in $Cd_{1-x}Cr_xSe$ and $Cd_{1-x}V_xSe$ (with very small x), respectively. Compared to the Mn-based III-V DMSs,[49] i.e., $Ga_{1-x}Mn_xAs$ and $In_{1-x}Mn_xAs$, which display ferromagnetism only up to 170 K, $Zn_{1-x}Cr_xTe$ ($x = 0.2$) shows it up to room temperature.[16,17] As an illustrative example for a potential spintronic application of such a semiconductor, we cite the strong resonant tunneling effect exploited in $Ga_{1-x}Mn_xAs$ as a magnetic tunnel transistor.[50]

[1] *Diluted Magnetic Semiconductors*, Semiconductors and Semimetals, edited by volume editors J. K. Furdyna and J. Kossut and series editors R. K. Willardson and A. C. Beer, Vol. 25 (Academic, San Diego, 1988).

[2] J. Blinowski, P. Kacman, and H. Przybylińska, Solid State Commun. **79**, 1021 (1991); J. Blinowski and P. Kacman, Phys. Rev. B **46**, 12298 (1992); J. Blinowski, P. Kacman, and J. A. Majewski, J. Cryst. Growth **159**, 972 (1996).

[3] A. K. Bhattacharjee, Phys. Rev. B **46**, 5266 (1992); **49**, 13987 (1994).

[4] W. Mac, Nguyen The Khoi, A. Twardowski, J. A. Gaj, and M. Demianiuk, Phys. Rev. Lett. **71**, 2327 (1993).

[5] W. Mac, A. Twardowski, and M. Demianiuk, Phys. Rev. B **54**, 5528 (1996).

[6] W. Mac, Nguyen The Khoi, A. Twardowski, and M. Demianiuk, J. Cryst. Growth **159**, 993 (1996).

[7] M. Herbich, W. Mac, A. Twardowski, K. Ando, Y. Shapira, and M. Demianiuk, Phys. Rev. B **58**, 1912 (1998).

[8] W. Mac, M. Herbich, A. Twardowski, and M. Demianiuk, Semicond. Sci. Technol. **15**, 748 (2000).

[9] H. Alawadhi, I. Miotkowski, V. Souw, M. McElfresh, A. K. Ramdas, and S. Miotkowska, Phys. Rev. B **63**, 155201 (2001).

[10] S. Tsoi, I. Miotkowski, S. Rodriguez, A. K. Ramdas, H. Alawadhi, and T. M. Pekarek, Phys. Rev. B **72**, 155207 (2005).

[11] X. Lu, I. Miotkowski, A. K. Ramdas, S. Rodriguez, H. Alawadhi, and T. M. Pekarek, Phys. Rev. B **76**, 035208 (2007).

[12] A. Twardowski, P. Glód, W. J. M. de Jonge, and M. Demianiuk, Solid State Commun. **64**, 63 (1987).

[13] W. Mac, A. Twardowski, P. J. T. Eggenkamp, H. J. M. Swagten, Y. Shapira, and M. Demianiuk, Phys. Rev. B **50**, 14144 (1994).

[14] T. M. Pekarek, J. E. Luning, I. Miotkowski, and B. C. Crooker, Phys. Rev. B **50**, 16914 (1994).

[15] T. M. Pekarek, I. Miotkowski, and B. C. Crooker, J. Appl. Phys. **79**, 6436 (1996).

[16] H. Saito, V. Zayets, S. Yamagata, and K. Ando, Phys. Rev. Lett. **90**, 207202 (2003).

[17] H. Saito, V. Zayets, S. Yamagata, and K. Ando, J. Appl. Phys. **93**, 6796 (2003).

[18] S. A. Wolf, D. D. Awschalom, R. A. Buhrman, J. M. Daughton, S. von Molnár, M. L. Roukes, A. Y. Chtchelkanova, and D. M. Treger, Science **294**, 1488 (2001).

[19] S. Tsoi, I. Miotkowski, S. Rodriguez, A. K. Ramdas, H. Alawadhi, and T. M. Pekarek, Phys. Rev. B **69**, 035209 (2004).

[20] C. Parks, Ph.D. thesis, Purdue University, 1994.

[21] M. Villeret, S. Rodriguez, and E. Kartheuser, Phys. Rev. B **41**, 10028 (1990).

[22] X. Lu, S. Tsoi, I. Miotkowski, S. Rodriguez, A. K. Ramdas, and H. Alawadhi, Phys. Rev. B **75**, 155206 (2007).

[23] J. T. Vallin, G. A. Slack, S. Roberts, and A. E. Hughes, Phys. Rev. B **2**, 4313 (1970).

[24] M. E. J. Boonman, W. Mac, A. Twardowski, A. Wittlin, P. J. M. van Bentum, J. C. Maan, and M. Demianiuk, Phys. Rev. B **61**, 5358 (2000).

[25] A. Twardowski, D. Heiman, M. T. Liu, Y. Shapira, and M. Demianiuk, Phys. Rev. B **53**, 10728 (1996).

[26] J. T. Vallin and G. D. Watkins, Phys. Rev. B **9**, 2051 (1974).

[27] J. Dieleman, R. S. Title, and W. V. Smith, Phys. Lett. **1**, 334 (1962).

[28] P. H. Kasai and Y. Otomo, Phys. Rev. Lett. **7**, 17 (1961).

[29] R. S. Title, Phys. Rev. **131**, 623 (1963).

[30] H. D. Fair, R. D. Ewing, and F. E. Williams, Phys. Rev. **144**, 298 (1966).

[31] T. Buch, B. Clerjaud, B. Lambert, and P. Kovacs, Phys. Rev. B **7**, 184 (1973).

[32] M. Godlewski and M. Kamińska, J. Phys. C **13**, 6537 (1980).

[33] R. S. Title, Phys. Rev. **133**, A1613 (1964).

[34] T. L. Estle and W. C. Holton, Phys. Rev. **150**, 159 (1966).

[35] G. W. Ludwig and M. R. Lorenz, Phys. Rev. **131**, 601 (1963).

[36] R. Rai, J. Y. Savard, and B. Tousignant, Phys. Lett. A **25**, 443 (1967).

[37] H. J. von Bardeleben, J. C. Launay, and V. Mazoyer, Appl. Phys. Lett. **63**, 1140 (1993).

[38] R. N. Schwartz, M. Ziari, and S. Trivedi, Phys. Rev. B **49**, 5274 (1994).

[39] J. Kreissl, K. Irmscher, P. Peka, M. U. Lehr, H. J. Schulz, and U. W. Pohl, Phys. Rev. B **53**, 1917 (1996).

[40] P. Christmann, B. K. Meyer, J. Kreissl, R. Schwarz, and K. W. Benz, Phys. Rev. B **53**, 3634 (1996).

[41] P. A. Slodowy and J. M. Baranowski, Phys. Status Solidi B **49**, 499 (1972).

[42] P. Peka, H. R. Selber, H.-J. Schulz, R. Schwarz, and K. W. Benz, Solid State Commun. **98**, 677 (1996).

[43] G. Goetz, U. W. Pohl, and H.-J. Schulz, J. Phys.: Condens. Matter **4**, 8253 (1992).

[44] D. L. Peterson, D. U. Bartholomew, U. Debska, A. K. Ramdas, and S. Rodriguez, Phys. Rev. B **32**, 323 (1985).

[45] C. H. Henry, K. Nassau, and J. W. Shiever, Phys. Rev. B **4**, 2453 (1971).

[46] P. Y. Yu and C. Hermann, Phys. Rev. B **23**, 4097 (1981).

[47] D. Wolverson, P. J. Boyce, C. M. Townsley, B. Schlichtherle, and J. J. Davies, J. Cryst. Growth **159**, 229 (1996).

[48] D. Heiman, P. A. Wolff, and J. Warnock, Phys. Rev. B **27**, 4848 (1983).

[49] S. Ohya, K. Ohno, and M. Tanaka, Appl. Phys. Lett. **90**, 112503 (2007).

[50] Y. Mizuno, S. Ohya, P. N. Hai, and M. Tnanka, Appl. Phys. Lett. **90**, 162505 (2007).